

Laser-Induced Reduction of Graphene Oxide by Intensity-Modulated Line Beam for Supercapacitor Applications

Tung Xuan Tran,[†] Hayelin Choi,[†] Cuong Huu Che,[†] Ji Hwan Sul,[‡] In Gyoo Kim,[‡] Seung-Mo Lee,[§] Jae-Hyun Kim,[§] and Jung Bin In^{*,†,ID}

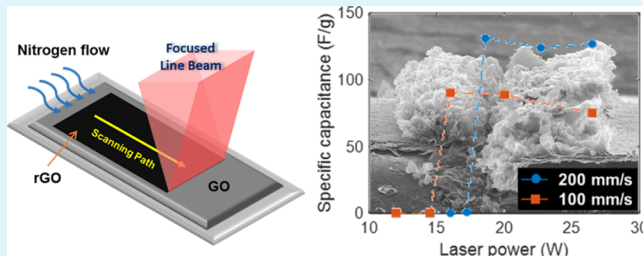
[†]Laser Thermal Nanoengineering Laboratory, School of Mechanical Engineering, Chung-Ang University, Seoul 06974, Republic of Korea

[‡]ICT Materials & Components Research Laboratory, Electronics and Telecommunications Research Institute (ETRI), Daejeon 34129, Republic of Korea

[§]Department of Nanomechanics, Korea Institute of Machinery and Materials, Daejeon 34113, Republic of Korea

Supporting Information

ABSTRACT: Supercapacitors are irreplaceable energy-storage devices for high power output and rapid charge/discharge of electrical energy. In this study, the laser-based fabrication of reduced graphene oxide (rGO) electrodes for supercapacitors is demonstrated with several new features of laser irradiation. A conventional CO₂ laser irradiation system is equipped with (1) a nitrogen blower to avoid combustion of the GO paper, (2) a cylindrical lens for producing a wide line beam, and (3) an optical chopper system for generating an intensity-modulated laser beam. Scanning of the intensity-modulated line beam transforms an extended area of GO into chemically reduced and physically porous graphene. The effects of the laser beam modifications and scanning parameters on the electrochemical performance of the rGO electrode are investigated. The rGO electrode exhibits a high specific capacitance (up to ~130 F/g) at a current density of 1 A/g. This work can serve as a reference for the process optimization of laser-induced GO reduction.



KEYWORDS: *laser-induced reduction, reduced graphene oxide, supercapacitor, EDLC, laser*

1. INTRODUCTION

Graphene has attracted significant attention as a promising electrode material for flexible energy-storage devices. Supercapacitors store electrical energy via rapid and reversible adsorption/desorption of electrolyte ions at the electrode surface.^{1,2} Owing to the exceptional physical, chemical, and electronic properties,^{3–8} graphene has been widely considered as a promising material for the active electrode of supercapacitors. Graphene films can be produced via mechanical exfoliation of highly ordered pyrolytic graphite,⁹ epitaxial growth,^{10–12} and growth on transition metal substrates by chemical vapor deposition (CVD).^{13,14} The metal catalyst-based CVD has been widely adopted especially for the large-area growth of few-layer graphene films. Thin Ni films¹⁴ and Cu foils¹⁵ are popular substrates that catalytically decompose hydrocarbon precursors and produce high-quality graphene layers.¹⁶ The graphene film can be transferred to other substrates by using various dry or wet transfer techniques.^{14,17,18} However, the high complexity and relatively low productivity of these methods have limited the real-world applications of graphene films for supercapacitors.

Graphene films may also be formed via the reduction of graphene oxide (GO). GO can be produced economically from graphite oxide on a large scale. Owing to its hydrophilicity, GO

can be evenly dispersed in solvents, such as water and alcohols. Thus, GO films can be easily produced by coating the solution on a substrate. The reduction of GO mainly involves decomposition and the subsequent removal of oxygen-containing groups (OCGs) contained in GO.¹⁹ In general, the quality of the reduced GO (rGO) is not as high as that of pristine graphene because of incomplete reduction, defects, and chemical residues involved in the reduction process. However, the successful use of rGO electrodes for high-performance supercapacitors has been demonstrated in many studies.^{20–23}

The laser-induced reduction of GO has been actively investigated because it has several technical advantages over other chemical or thermal methods.^{20,24–26} Studies have shown that the light emitting from various light sources characterized by a wide range of wavelengths (from UV to microwave) can successfully reduce GO without the use of a reducing chemical agent.^{22,27,28} Compared with other high-intensity light sources such as flash lamps,^{29,30} lasers yield more efficient reduction of GO. The extremely high energy density

Received: August 25, 2018

Accepted: October 29, 2018

Published: October 29, 2018

of a focused laser beam enables instant reduction of a GO film under ambient conditions. Lasers generally have higher energy efficiencies than flash lamps. Furthermore, the programmed scanning of the focused beam can easily produce an rGO pattern (even on a micrometer scale) without a photomask, which is preferable in the fabrication of planar micro-supercapacitors.^{31,32}

However, because of the small diameter of the focused beam, large-scale laser reduction of GO films (where a large area of GO is scanned) may require significant processing time. Moreover, systematic investigations considering the effect of laser scanning parameters on the electrochemical performance of rGO films are lacking. Factors such as the laser power, scanning speed, and laser-exposure duration can affect the structural morphology and the chemical composition of the rGO. In fact, these factors determine the capacitance, which is one of the most important metrics for the evaluation of supercapacitors.

To address these issues, in this study, high-throughput laser reduction of GO paper was achieved by employing a line beam of a CO₂ laser. For increased productivity of laser processing, line-shaped laser beams have been widely adopted in various applications such as laser crystallization,³³ sintering of nanoparticles,³⁴ and surface structuring.³⁵ Compared with a small-diameter point beam, the width of a line beam is significantly extended, resulting in shorter processing time per unit irradiation area. In our work, this wide line beam enabled large-area reduction of GO in a single stroke of scanning. The laser-rGO films were assembled into sandwich-type supercapacitors, and their electrochemical characteristics were determined. The CO₂ laser was equipped with a nitrogen gas blower and a mechanical beam chopper, to determine the effect of an intensity-modulated laser beam on the performance of rGO supercapacitor electrodes. The effect of various laser scanning parameters on the capacitance of supercapacitors was also determined.

2. EXPERIMENTAL SECTION

2.1. Preparation of Graphene Oxide Paper and Laser Reduction. GO paper was prepared by bar-coating a GO slurry (density: 25 g/L, Grapheneall Co.) on a polyethylene terephthalate (PET) film. The coated film (thickness: 16–18 μm) was dried for 24 h under ambient conditions and then carefully peeled from the PET film. The atomic carbon to oxygen (C/O) ratio of the as-prepared GO paper was ~2.24 (Table 1). The GO paper was reduced using a

Table 1. Elemental Composition Measured by XPS

sample #	scanning parameter	carbon (%)	oxygen (%)	C/O ratio
GO		69.09	30.83	2.24
7 (top)	26.5 W 200 mm/s	90.85	9.15	9.93
7 (bottom)	26.5 W 200 mm/s	83.7	16.3	5.13
8 (top)	18.6 W 200 mm/s	88.57	11.43	7.75
9 (top)	26.5 W 100 mm/s	96.39	3.61	26.70

conventional CO₂ laser engraver (C40-60W, wavelength: 10.6 μm, Coryart). The original system was modified to obtain a line beam. A plano-convex round cylindrical lens (LJ7003RM-G, $f = 50.0$ mm, Thorlabs) was adopted, and its plano axis was aligned vertical to the direction of laser beam scanning. Measurements via the knife-edge method yielded a beam size of 3.9×0.23 mm² ($1/e^2$ width of a Gaussian beam). The lens assembly was equipped with a gas nozzle (NZAK1-0.6, Misumi) for blowing nitrogen gas toward the beam spot and providing an almost inert ambience for laser reduction. During laser irradiation, the flow rate was set to ~10 L/min. An intensity-

modulated laser beam was generated by installing a mechanical beam chopper (MC2000B-EC, Thorlabs) at the aperture of the laser. The chopper wheel (MC1F10HP, Thorlabs) enabled a 50% duty cycle, where 50% of the laser power was delivered to the GO surface. The laser power was measured using a power meter (Nova II, P/N 7Z01550, Ophir) combined with a power sensor (30(150)A-BB-18 P/N 7Z02699, Ophir).

2.2. Characterization of rGO. The micromorphology of rGO was observed via field-emission scanning electron microscopy (FE-SEM; SIGMA, Carl Zeiss). The elemental composition of the rGO was determined via energy-dispersive X-ray spectroscopy (EDX; NORAN System 7, Thermo Fisher Scientific) and by X-ray photoelectron spectroscopy (XPS; K-alpha Plus, Thermo Fisher Scientific). The EDX data were used for the mapping of the carbon and oxygen compositions. Furthermore, the C/O ratio was calculated from the XPS data. Raman spectra of rGO were obtained using a confocal Raman microscope (inVia, Renishaw). The wavelength and spot diameter of the Raman laser were 514 nm and ~5 μm, respectively.

2.3. Supercapacitor Fabrication and Electrochemical Measurements. An electrochemical test cell (ECC-Aqu, EL-CELL GmbH) was used to evaluate the electrochemical performance of the rGO electrodes. A large piece of rGO film was produced via raster scanning (line pitch: 3 mm) with the laser beam. Video S1 shows the scanning process. For the preparation of symmetric anode and cathode electrodes, each rGO film was cut into two identical pieces. The as-prepared rGO films were then loaded on gold current collector disks and placed inside the test cell. A glass-fiber membrane (ECC1-01-0012-C/L, EL-CELL GmbH) was inserted between the disks as a separator. The positioning was such that the top surface (or irradiated surface) of the rGO faced the separator. This capacitor assembly was soaked with 500 μL of a 1 M H₂SO₄ electrolyte solution (ACS reagent grade, Sigma-Aldrich). Figure S1 of the Supporting Information shows an illustration of the capacitor structure. Prior to the electrochemical tests, the capacitor was left undisturbed for 90 min to allow sufficient wetting of the electrodes. An electrochemical instrument (SP-150, Bio-Logic Science Instruments) was used to perform cyclic voltammetry (CV) and galvanostatic charge/discharge testing. The specific capacitance values were calculated from the equations provided in the Supporting Information.

3. RESULTS AND DISCUSSION

3.1. Laser Reduction of Graphene Oxide by Line Beam. CO₂ lasers have been extensively used for the efficient cutting or engraving of nonmetallic materials. Recently, many studies have shown that GO can be successfully reduced by irradiating a GO film with a CO₂ laser.^{21,22} The photothermal interaction leads to heating of the GO above a thermal threshold for reduction, whereas the photochemical interaction can directly affect the chemical bond between the graphene and OCGs, resulting in a nonthermal reduction.²⁸ Considering the long wavelength of the CO₂ laser and the relatively large thickness of the GO film, the absorption-induced photothermal heating plays a major role in the reduction of GO. Here, a CO₂ laser irradiation system with flying optics was employed for GO reduction. In addition, the laser system was modified to generate pulses of a line beam for enhanced reduction of GO.

The schematic in Figure 1a shows the laser-reduction processes of GO paper by scanning with a point beam and a line beam of the CO₂ laser. The photograph in Figure 1b shows the lens assembly. As-prepared freestanding GO paper was placed on a glass slide and then reduced via irradiation with a line beam of the CO₂ laser. Owing to rapid heating and cooling, the scanning of a focused laser beam can successfully reduce GO under ambient conditions. However, when relatively thick GO paper was irradiated in air with a high-

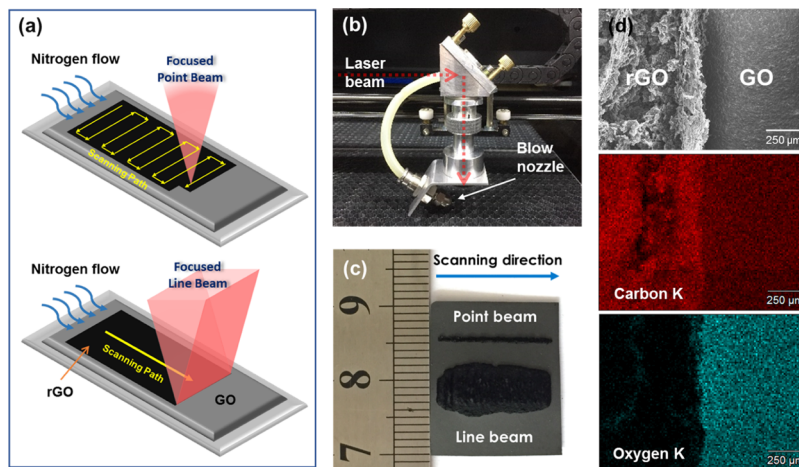


Figure 1. (a) Schematic showing GO-film laser reduction by a point beam and a line beam. Photograph showing the (b) focusing optics assembly and (c) comparison of single scanning performed with a point beam and a line beam. (d) SEM image of the rGO (left)/GO (right) interface. EDX element mapping of C and O at the interface.

power laser beam, the GO underwent combustion (see Figure S2 in Supporting Information). The CO₂ laser was therefore equipped with a nitrogen gas blower (see Figure 1b) to avoid combustion and provide the line beam spot with an inert ambience. The direction of laser scanning was always left-to-right, based on the coordinate system of the lens assembly shown in Figure 1b, and the nitrogen flow was also parallel to this direction. This flow also prevented contamination of the rGO and the focus lens by reduction by-products.

Upon irradiation with the line beam, the GO paper was instantly reduced and converted to a visually black porous material. Compared with a regular point beam focused through a plano-convex spherical lens, the extended line beam could reduce a significantly wider area of GO in a single stroke of scanning (Figure 1a). Figure 1c shows the considerable difference in width of the reduced areas. The width of the rGO reduced by the line beam (~5 mm) is comparable to the beam width (~3.9 mm). Figure 1d shows an SEM image and the corresponding EDX maps for carbon and oxygen at the interface of GO and rGO obtained via line beam irradiation. The EDX mapping results reveal a stark contrast in composition: a large carbon (brighter red area) to oxygen (darker area) ratio of the rGO indicates successful laser removal of the OCGs.

3.2. Laser Reduction of Graphene Oxide by an Intensity-Modulated Beam. To produce laser beam pulses, the intensity of the continuous wave (CW) CO₂ laser beam was modulated using an optical chopper system. As described in Figure 2a, the optical chopper wheel allows periodic transmission of the incident CW laser beam for a pulse duration (Δt), and the wheel rotation generates a train of laser pulses. The chopper wheel used in this study has a 50% duty cycle; hence, the on-state duration and the off-state duration are equal. In addition, the repetition rate, which indicates the frequency of the output pulses, can be controlled by adjusting the revolution speed of the wheel. The pulsed beam was focused into a line beam using the cylindrical lens.

As-prepared GO paper was irradiated with the modulated line beam by varying the pulse duration and the repetition rate. Figure 2b shows the modulation parameters and photographs of the rGO produced by the corresponding beam pulses. The upper and lower images show the top and the bottom surfaces,

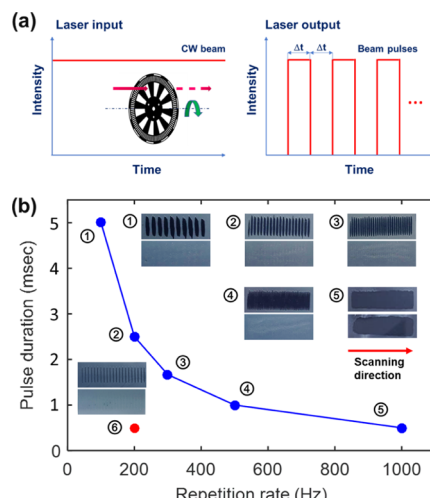


Figure 2. (a) Schematic showing the generation of the intensity-modulated CW laser. (b) Effect of the repetition rate and pulse duration of the laser pulses on the reduction of GO paper (scanning speed: 200 mm/s, laser power: 26.5 W). The upper and lower images show the top and the bottom surfaces, respectively, of the rGO paper.

respectively, of the rGO paper. A scanning speed and an output laser power of 200 mm/s and 26.5 W, respectively, were employed for each experiment. The rGO strip was scanned from the left to the right, as indicated by the arrow.

At low repetition rates (or frequencies) of laser pulses, the pulse duration is long. Thus, each laser pulse affects a large region of the GO surface. Low repetition rates also result in increased pulse-to-pulse distance, possibly leaving unreduced GO between pulse spots. As Figure 2b shows, each laser pulse reduced a relatively large area of the GO, yielding a discontinuous reduction pattern at low repetition rates of 100, 200, and 300 Hz (samples #1, #2, and #3, respectively). Reduction to the bottom surface of the GO was limited because of insufficient heat penetration, and only slightly heat-affected areas were visible.

In contrast, an almost continuous reduction strip was obtained at high repetition rates (500 and 1 kHz, samples #4 and #5), consistent with the overlapping of neighboring reduction spots. Consider the following conditions: pulse

duration: 0.5 ms, frequency: 1 kHz, scanning speed: 200 mm/s, and corresponding spot-to-spot distance: 200 μm . Thus, the width of a single pulse spot should be larger than the 200 μm pitch to obtain a continuous rGO strip. To measure the width of rGO reduced by a single pulse, GO paper was irradiated at 200 Hz (pulse duration: 0.5 ms) (sample #6). Indeed, the resulting width of the single spot (i.e., $\sim 260 \mu\text{m}$) was larger than the interspot distance (see Figure 3a).

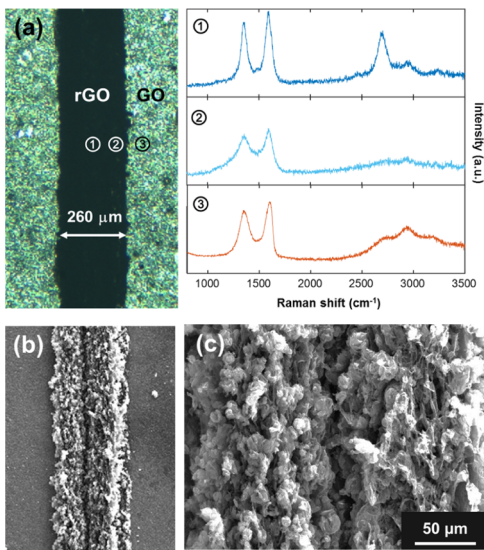


Figure 3. (a) Optical microscopy image of a single reduction spot in sample #6 (left) and Raman spectra obtained at the indicated positions (right). (b) SEM image of a single reduction spot. (c) High-magnification SEM image near the center of the spot line.

Figure 3a also shows the micro-Raman spectra corresponding to the positions denoted as ①, ②, and ③ in the optical microscopy image. The D band occurring at position ② is wider than the D band at position ①. A similar level of $I_{\text{D}}/I_{\text{G}}$ ratio was observed at position ② ($I_{\text{D}}/I_{\text{G}}$: 0.90) and position ① ($I_{\text{D}}/I_{\text{G}}$: 0.87). However, a distinct 2D band signifying the abundance of single-layer graphene occurred at position ①, as the intensity of the incident Gaussian laser beam is highest at the center. As shown in Figure 3b,c, this high intensity resulted in a deep ablation-induced groove at the spot center (see also Figure S3 of the Supporting Information).

The GO paper was reduced from the irradiated top to the bottom at 1 kHz (sample #5), but reduction to the bottom was unattainable by a single pulse of the same pulse duration (sample #6). This deeper reduction at 1 kHz can be attributed to unique optical and thermal characteristics of the overlap area corresponding to successive laser pulses. Absorption of rGO is higher than that of GO for the wavelength of the CO₂ laser (10.6 μm).³⁶ Thus, for overlapping beam spots, the subsequent laser beam was more efficiently absorbed (than in the case of nonoverlapping spots), especially on the previously reduced area. In addition, the absorbed heat can accumulate during scanning of the laser pulses at a relatively high repetition rate. Before the heat absorbed from the previous laser pulse dissipates, the subsequent laser pulse can irradiate the GO, leading to a further temperature increase at the GO paper/glass support interface. This phenomenon is typically observed in laser thermal processing. Therefore, the bottom-side reduction suggests that photothermal reduction prevails in the CO₂-laser reduction of the GO paper.

Figure 4 shows the microstructure of rGO paper, as observed via FE-SEM. Owing to explosive degassing of the reduction products, laser irradiation yields a significantly expanded and porous structure.²¹ Figure 4a shows the cross-sectional SEM image of rGO reduced to a shallow depth because of insufficient heat penetration. The GO layer persists underneath the rGO. However, the dense GO layer is absent from the fully reduced GO (Figure 4b). The images in Figure 4c–f show the difference in the morphology of rGO reduced by a CW laser beam (c,d) and a 1 kHz-pulsed beam (e,f) at powers of 14 (c,e) and 26.5 W (d,f). The pulsed beam produced rGO with visible traces of laser pulses (pulse-to-pulse pitch: 200 μm), whereas the CW beam produced a random structure. The additional characteristics (thickness, Raman spectrum, and electrical resistivity) of the rGO strips produced at different powers are provided in Figures S4 and S5 of the Supporting Information.

3.3. Influence of Laser Processing Parameters on Capacitance. The influence of laser power and scanning speed on the electrochemical performance of rGO paper was evaluated. A series of rGO films were prepared by varying the scanning parameters. Various laser powers were applied to the as-prepared GO films for fixed scanning speeds of 100 and 200 mm/s. The same line-beam pulses irradiated the GO at 1 kHz. Among the examined parameters, the highest capacitance (131 F/g at 1 A/g) was obtained at 18.6 W and 200 mm/s. The

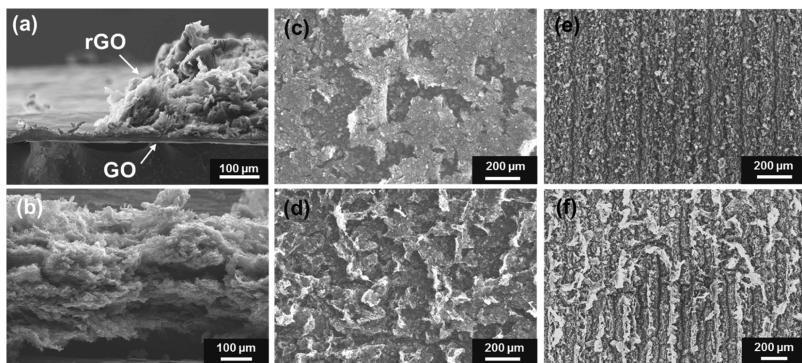


Figure 4. FE-SEM images of rGO. Cross-sectional SEM images revealing reductions of rGO (a) to a shallow depth and (b) throughout the film. Top-view SEM images of rGO reduced by scanning (c,d) a CW laser beam and (e,f) laser beam pulses (1 kHz) at (c,e) 14 and (d,f) 26.5 W and a speed of 200 mm/s.

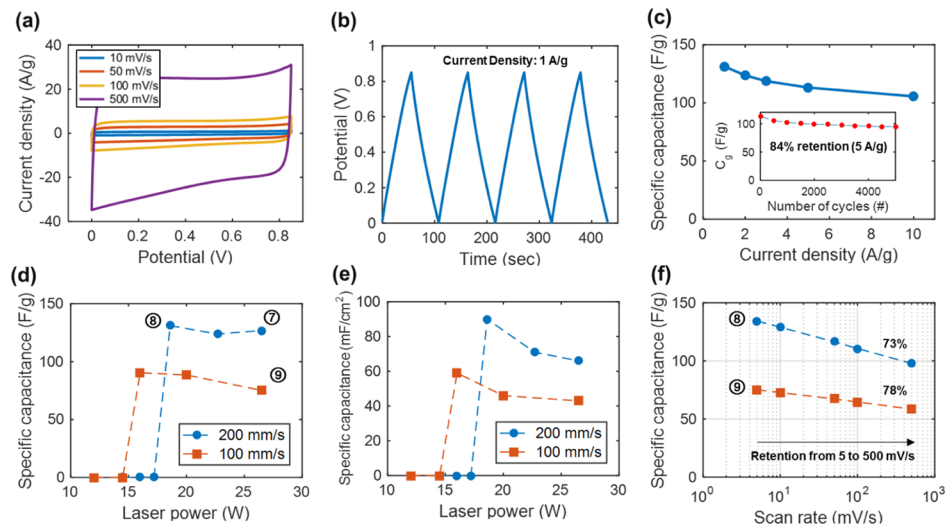


Figure 5. (a–c) Electrochemical characterization of rGO [sample denoted as #8 in (d)] reduced at 18.6 W and 200 mm/s. (a) CV curves at scan rates ranging from 10 to 500 mV/s, (b) four cycles of galvanostatic charge/discharge curves at 1 A/g, and (c) gravimetric capacitance (C_g) calculated from the galvanostatic charge/discharge (CC) curves at different current densities. The inset of (c) shows the result of the 5000 CC cycles at 5 A/g. (d,e) C_g and areal capacitance (C_A), respectively, calculated from the CC curves (current density: 1 A/g) obtained at different laser powers and scanning speeds. (f) Gravimetric capacitance of rGO [denoted as samples #8 and #9 in (d)] calculated from the CV curves obtained at different scan rates.

electrochemical characteristics of the rGO film are shown in Figure 5a–c. Figure 5a,b shows a series of pseudorectangular CV curves of the rGO at various scan rates and four cycles of almost triangular galvanostatic charge/discharge curves at 1 A/g, respectively. Both features correspond to typical behaviors of electrical double-layer capacitors. Figure 5c reveals that the capacitance was retained up to a high current density of 10 A/g, indicating the high-power performance of the rGO electrode. The inset of Figure 5c shows the result of a repetitive charge/discharge test (5000 cycles), where a retention of 84% was obtained.

Figure 5d,e shows the specific capacitance (Figure 5d: gravimetric capacitance in F/g; Figure 5e: areal capacitance in mF/cm^2) of the rGO electrodes that were prepared by varying the laser power and the scanning speed. The capacitance was calculated from the discharge slopes of the galvanostatic charge/discharge curves at a current density of 1 A/g. Furthermore, the areal capacitance was calculated from the macroscopic area of a single electrode. The laser power was directly measured at the film position by a power sensor. Therefore, the power value indicates the actual dose of the intensity-modulated laser beam.

Figure 5d reveals unexpected effects of the laser power on the capacitance: the specific capacitance increases abruptly at the threshold power and changes moderately or even decreases at larger doses of laser light. Below the threshold, the GO paper was only partially reduced, as evidenced by an unreduced bottom surface (see Figure 2b). The capacitance of the partially reduced GO was very small. Moreover, when the power was slightly lower than the threshold, the reduction was nonreproducible, sometimes resulting in a nonuniform rGO area. In this case, the capacitance value was considered insignificant and was therefore excluded from the data. Above the threshold, the GO paper became completely black to the bottom, indicative of significant reduction. A higher threshold power was observed at a scanning speed of 200 mm/s than at 100 mm/s.

However, the gravimetric capacitance did not change appreciably when the laser power was increased further. We attribute this to the two counteractive effects of increasing laser power on the reduction. The GO directly exposed to the strong incident laser light can be removed by ablation, resulting in a decreased mass loading of the electrode. The decrease in the areal capacitance (calculated based on the single-electrode area) with laser power reflects this material removal (Figure 5e). Researchers found that the gravimetric capacitance of the supercapacitors assembled with the identical electrode material can significantly increase as its mass loading (mg/cm^2) decreases.³⁷ Therefore, the light rGO electrode produced by a high-intensity laser beam could exhibit an increased gravimetric capacitance.

In addition, compared with a lower-power laser, a higher-power laser enables greater reduction at the bottom of the GO paper. Laser irradiation of our relatively thick GO film yielded a nonuniform reduction along the thickness direction. For instance, C/O atomic ratios of ~9.93 and ~5.13 were measured (via XPS) at the top surface and the bottom surface, respectively, of the rGO film reduced at 26.5 W and 200 mm/s (Table 1). As previously mentioned, limited light and heat penetrations occur along the out-of-plane direction associated with the stacked GO layers. Thus, a significant temperature gradient probably occurs during laser irradiation, with the highest temperature at the top of the film and the lowest temperature at the bottom. The depth of the reduction front will therefore extend to the bottom of the GO paper when the laser power is increased, which, on the one hand, is preferable for increased capacitance.

On the other hand, the GO directly exposed to the strong incident laser light can be heated excessively, thereby adversely affecting the capacitance of rGO. Several studies determined the effect of increasing reduction temperature on the electrochemical performance of rGO.^{26,38} The results revealed that, compared with annealing of GO at a lower temperature (250 °C), annealing at a higher temperature (1000 °C) produces rGO exhibiting better chemical reduction, but

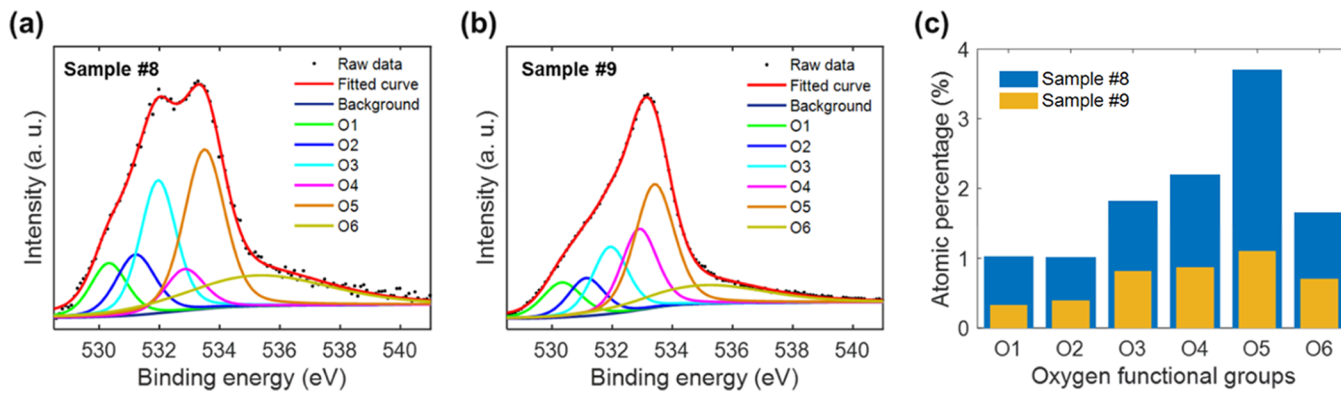


Figure 6. XPS O 1s peak spectra of (a) sample #8 (18.6 W, 200 mm/s) and (b) sample #9 (26.5 W, 100 mm/s). OCGs are labeled from O1 to O5 (O1: quinone, O2: C=O-OH, O3: C=O, O4: C-O, O5: C-OH). O6 denotes adsorbed water or oxygen.^{38,39} (c) Atomic percentages of the OCGs for samples #8 and #9.

markedly lower capacitance because of pseudocapacitive OCG removal. Their findings support our argument that laser irradiation at a high power can lead to a decrease in the capacitance of rGO.

At a scanning speed of 100 mm/s, the GO surface was irradiated with more pulses (than at 200 mm/s), and the stronger thermal effect on the rGO yielded a greater decrease in the capacitance (Figure 5d). Instead, the rGO reduced at a higher temperature (or scanned at a higher power and a slower beam motion) exhibited higher capacitance retention (compared with the rGO reduced at lower temperature) at high scan rates. This is attributed to the slow charge/discharge kinetics of the redox reactions involving OCGs.²⁶ For example, the retention rates from 5 to 500 mV/s are 73 and 78% for 18.6 W and 200 mm/s (sample #8) and 26.5 W and 100 mm/s (sample #9), respectively (Figure 5f). The electrochemical impedance spectroscopy (EIS) results of samples #8 and #9 are provided in Figure S6 of the Supporting Information. The C/O ratio (associated with the degree of reduction) of sample #9 is significantly higher than that of sample #8 (Table 1). Figure 6a,b shows the XPS O 1s peak spectra of samples #8 and #9, respectively. Each spectrum was deconvoluted to elemental peaks, which signify the existence of specific OCGs, via curve fitting.^{26,38–40} The signals of OCGs, especially quinone (O1) and carbonyl (O3) that are responsible for pseudocapacitance in acidic electrolytes,^{26,38} are more suppressed for sample #9 compared with sample #8. Figure 6c shows the atomic percentages of the OCGs calculated from the elemental peaks, revealing decreased contents of quinone and carbonyl groups in sample #9.

Another series of rGO films were prepared using the CW laser beam (scanning speed: 200 mm/s), and the effect of the modulated laser was compared with that of the CW laser. The power of the CW laser beam was adjusted (to 26.5, 29.5, and 33.5 W), so that areal densities (or mass loadings) of the rGO films comparable to those of the rGO produced by the modulated beam were realized. Compared with the modulated beam, the CW beam produced an rGO with a lower specific capacitance (see Figure 7). The enhanced capacitance induced by the modulated beam may have resulted from a laterally nonuniform degree of reduction, as suggested in Figure 3. The pseudocapacitive OCGs could survive on the peripheral area of each pulse spot, thereby contributing to the increased capacitance. Meanwhile, the spot center was highly reduced and could therefore provide an efficient electrical conduction

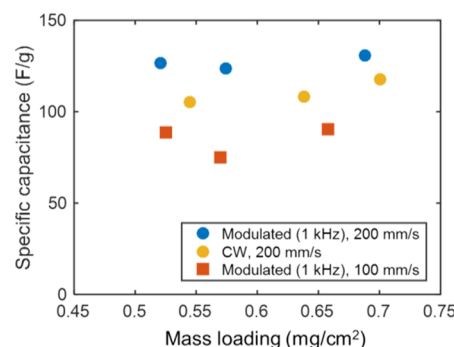


Figure 7. Specific capacitance (F/g) of rGO electrodes produced by the CW laser beam and the intensity-modulated beam.

path to the current collector. The spot centers were closely placed for modulated beam scanning at 100 mm/s. Thus, the OCGs that survived from the previous beam pulse were removed by the overlapping beam pulses, resulting in decreased capacitance. The CV curves of the samples shown in Figure 7 are provided in Figure S7 of the Supporting Information.

Although extraordinary capacitance values of laser-rGO have been reported, the performance comparison should be conducted based on practical metrics.^{41,42} As aforementioned, the gravimetric capacitance tends to increase as the mass loading (mg/cm^2) decreases.³⁷ In this respect, the capacitance of our rGO is comparable to the values (130–140 F/g in an aqueous electrolyte) recently reported by Yang et al.²³ The mass loading of their rGO electrode was $0.25 \text{ mg}/\text{cm}^2$, which is less than a half of our mass loadings. However, they used an excimer laser to reduce the GO dispersed in water, whereas dry GO paper was reduced in our study using a relatively economical CO_2 laser under ambient conditions. Moreover, compared with their cyclic stability (47%), our rGO electrode exhibited a markedly higher capacitance retention (84%).

The rGO produced by laser-induced reduction of GO is comparable with the laser-induced graphene (LIG) that is derived from a polymer precursor. Recently, researchers demonstrated that laser irradiation of a polymer such as polyimide (PI) produces porous LIG.^{32,43} The LIG was also successfully applied to supercapacitor electrodes. However, our rGO electrode exhibits a higher areal capacitance than LIG electrodes ($\sim 10 \text{ mF}/\text{cm}^2$).⁴⁴ Moreover, the thermal reduction of GO occurs at a lower temperature ($\sim 190^\circ\text{C}$) than the

pyrolysis of PI ($\sim 550^\circ\text{C}$).⁴³ Therefore, when a graphene precursor should be irradiated on a thermally unstable substrate with a laser beam, the laser-induced GO reduction may be preferred to the LIG formation process.

4. CONCLUSIONS

In summary, high-throughput reduction of GO paper has been realized by employing an intensity-modulated line beam of a CO₂ laser under a nitrogen flow. The wide beam swept a large area, instantly converting the irradiated GO to highly swollen and porous rGO. The produced rGO film was used for the electrode of supercapacitors. The influence of the laser power and scanning speed on the performance of the rGO electrode was determined. The results revealed that once the laser dose exceeds the threshold for through-thickness reduction, a lower laser power and a faster scanning are preferable for increased capacitance. Our findings offer a fundamental base for an optimal reduction process of relatively thick GO paper that is essential for low-cost and large-scale production of high-performance rGO films.

■ ASSOCIATED CONTENT

Supporting Information

The Supporting Information is available free of charge on the ACS Publications website at DOI: [10.1021/acsami.8b14678](https://doi.org/10.1021/acsami.8b14678).

Calculation of specific capacitance, cross-sectional SEM image of a reduction spot, Raman spectra of rGO, dimensions and resistivity of rGO strips, EIS plots of rGO electrodes, and CV curves of the Figure 7 samples ([PDF](#))

Laser reduction processing ([AVI](#))

■ AUTHOR INFORMATION

Corresponding Author

*E-mail: jbin@cau.ac.kr

ORCID

Jung Bin In: [0000-0002-9418-9873](https://orcid.org/0000-0002-9418-9873)

Notes

The authors declare no competing financial interest.

■ ACKNOWLEDGMENTS

We gratefully acknowledge the financial support from the R&D Convergence Program of MSIT (Ministry of Science and ICT) and NST (National Research Council of Science & Technology) of the Republic of Korea (Grant CAP-13-02-ETRI). This work was also supported by the Basic Science Research Program (no. NRF-2015R1C1A1A01052523) and Nano-Material Technology Development Program (no. NRF-2016M3A7B4910532) through the National Research Foundation of Korea (NRF) grant funded by the Korea government (MSIT).

■ REFERENCES

- (1) Simon, P.; Gogotsi, Y. Materials for Electrochemical Capacitors. *Nat. Mater.* **2008**, *7*, 845–854.
- (2) Miller, J. R.; Simon, P. Materials Science - Electrochemical Capacitors for Energy Management. *Science* **2008**, *321*, 651–652.
- (3) Stoller, M. D.; Park, S.; Zhu, Y.; An, J.; Ruoff, R. S. Graphene-Based Ultracapacitors. *Nano Lett.* **2008**, *8*, 3498–3502.
- (4) Geim, A. K. Graphene: Status and Prospects. *Science* **2009**, *324*, 1530–1534.

(5) Bolotin, K. I.; Sikes, K. J.; Jiang, Z.; Klima, M.; Fudenberg, G.; Hone, J.; Kim, P.; Stormer, H. L. Ultrahigh Electron Mobility in Suspended Graphene. *Solid State Commun.* **2008**, *146*, 351–355.

(6) Zhang, Y.; Tan, Y.-W.; Stormer, H. L.; Kim, P. Experimental Observation of the Quantum Hall Effect and Berry's Phase in Graphene. *Nature* **2005**, *438*, 201–204.

(7) Lee, C.; Wei, X.; Kysar, J. W.; Hone, J. Measurement of the Elastic Properties and Intrinsic Strength of Monolayer Graphene. *Science* **2008**, *321*, 385–388.

(8) Balandin, A. A.; Ghosh, S.; Bao, W.; Calizo, I.; Teweldebrhan, D.; Miao, F.; Lau, C. N. Superior Thermal Conductivity of Single-Layer Graphene. *Nano Lett.* **2008**, *8*, 902–907.

(9) Novoselov, K. S.; Geim, A. K.; Morozov, S. V.; Jiang, D.; Zhang, Y.; Dubonos, S. V.; Grigorieva, I. V.; Firsov, A. A. Electric Field Effect in Atomically Thin Carbon Films. *Science* **2004**, *306*, 666–669.

(10) Winterlin, J.; Bocquet, M.-L. Graphene on Metal Surfaces. *Surf. Sci.* **2009**, *603*, 1841–1852.

(11) Land, T. A.; Michely, T.; Behm, R. J.; Hemminger, J. C.; Comsa, G. STM Investigation of Single Layer Graphite Structures Produced on Pt(111) by Hydrocarbon Decomposition. *Surf. Sci.* **1992**, *264*, 261–270.

(12) Berger, C.; Song, Z.; Li, X.; Wu, X.; Brown, N.; Naud, C.; Mayou, D.; Li, T.; Hass, J.; Marchenkov, A. N.; Conrad, E. H.; First, P. N.; de Heer, W. A. Electronic Confinement and Coherence in Patterned Epitaxial Graphene. *Science* **2006**, *312*, 1191–1196.

(13) Zhang, Y.; Zhang, L.; Zhou, C. Review of Chemical Vapor Deposition of Graphene and Related Applications. *Acc. Chem. Res.* **2013**, *46*, 2329–2339.

(14) Kim, K. S.; Zhao, Y.; Jang, H.; Lee, S. Y.; Kim, J. M.; Kim, K. S.; Ahn, J.-H.; Kim, P.; Choi, J.-Y.; Hong, B. H. Large-Scale Pattern Growth of Graphene Films for Stretchable Transparent Electrodes. *Nature* **2009**, *457*, 706–710.

(15) Li, X.; Cai, W.; An, J.; Kim, S.; Nah, J.; Yang, D.; Piner, R.; Velamakanni, A.; Jung, I.; Tutuc, E.; Banerjee, S. K.; Colombo, L.; Ruoff, R. S. Large-Area Synthesis of High-Quality and Uniform Graphene Films on Copper Foils. *Science* **2009**, *324*, 1312–1314.

(16) Li, X.; Cai, W.; Colombo, L.; Ruoff, R. S. Evolution of Graphene Growth on Ni and Cu by Carbon Isotope Labeling. *Nano Lett.* **2009**, *9*, 4268–4272.

(17) Suk, J. W.; Kitt, A.; Magnuson, C. W.; Hao, Y.; Ahmed, S.; An, J.; Swan, A. K.; Goldberg, B. B.; Ruoff, R. S. Transfer of Cvd-Grown Monolayer Graphene onto Arbitrary Substrates. *ACS Nano* **2011**, *5*, 6916–6924.

(18) Bae, S.; Kim, H.; Lee, Y.; Xu, X.; Park, J.-S.; Zheng, Y.; Balakrishnan, J.; Lei, T.; Kim, H. R.; Song, Y. I.; Kim, Y.-J.; Kim, K. S.; Özyilmaz, B.; Ahn, J.-H.; Hong, B. H.; Iijima, S. Roll-to-Roll Production of 30-Inch Graphene Films for Transparent Electrodes. *Nat. Nanotechnol.* **2010**, *5*, 574–578.

(19) Loh, K. P.; Bao, Q.; Eda, G.; Chhowalla, M. Graphene Oxide as a Chemically Tunable Platform for Optical Applications. *Nat. Chem.* **2010**, *2*, 1015–1024.

(20) El-Kady, M. F.; Strong, V.; Dubin, S.; Kaner, R. B. Laser Scribing of High-Performance and Flexible Graphene-Based Electrochemical Capacitors. *Science* **2012**, *335*, 1326–1330.

(21) Gao, W.; Singh, N.; Song, L.; Liu, Z.; Reddy, A. L. M.; Ci, L.; Vajtai, R.; Zhang, Q.; Wei, B.; Ajayan, P. M. Direct Laser Writing of Micro-Supercapacitors on Hydrated Graphite Oxide Films. *Nat. Nanotechnol.* **2011**, *6*, 496–500.

(22) Bhattacharjya, D.; Kim, C.-H.; Kim, J.-H.; You, I.-K.; In, J. B.; Lee, S.-M. Fast and Controllable Reduction of Graphene Oxide by Low-Cost CO₂ Laser for Supercapacitor Application. *Appl. Surf. Sci.* **2018**, *462*, 353–361.

(23) Yang, D.; Bock, C. Laser Reduced Graphene for Supercapacitor Applications. *J. Power Sources* **2017**, *337*, 73–81.

(24) Chua, C. K.; Pumera, M. Chemical Reduction of Graphene Oxide: A Synthetic Chemistry Viewpoint. *Chem. Soc. Rev.* **2014**, *43*, 291–312.

(25) Sofer, Z.; Jankovský, O.; Šimek, P.; Sedmidubský, D.; Šturala, J.; Kosina, J.; Mikšová, R.; Macková, A.; Mikulics, M.; Pumera, M.

Insight into the Mechanism of the Thermal Reduction of Graphite Oxide: Deuterium-Labeled Graphite Oxide Is the Key. *ACS Nano* **2015**, *9*, 5478–5485.

(26) Chen, C.-M.; Zhang, Q.; Yang, M.-G.; Huang, C.-H.; Yang, Y.-G.; Wang, M.-Z. Structural Evolution During Annealing of Thermally Reduced Graphene Nanosheets for Application in Supercapacitors. *Carbon* **2012**, *50*, 3572–3584.

(27) Chen, W.; Yan, L.; Bangal, P. R. Preparation of Graphene by the Rapid and Mild Thermal Reduction of Graphene Oxide Induced by Microwaves. *Carbon* **2010**, *48*, 1146–1152.

(28) Arul, R.; Oosterbeek, R. N.; Robertson, J.; Xu, G.; Jin, J.; Simpson, M. C. The Mechanism of Direct Laser Writing of Graphene Features into Graphene Oxide Films Involves Photoreduction and Thermally Assisted Structural Rearrangement. *Carbon* **2016**, *99*, 423–431.

(29) Cote, L. J.; Cruz-Silva, R.; Huang, J. Flash Reduction and Patterning of Graphite Oxide and Its Polymer Composite. *J. Am. Chem. Soc.* **2009**, *131*, 11027–11032.

(30) Park, S.-H.; Kim, H.-S. Environmentally Benign and Facile Reduction of Graphene Oxide by Flash Light Irradiation. *Nanotechnology* **2015**, *26*, 205601.

(31) El-Kady, M. F.; Kaner, R. B. Scalable Fabrication of High-Power Graphene Micro-Supercapacitors for Flexible and on-Chip Energy Storage. *Nat. Commun.* **2013**, *4*, 1475.

(32) In, J. B.; Hsia, B.; Yoo, J.-H.; Hyun, S.; Carraro, C.; Maboudian, R.; Grigoropoulos, C. P. Facile Fabrication of Flexible All Solid-State Micro-Supercapacitor by Direct Laser Writing of Porous Carbon in Polyimide. *Carbon* **2015**, *83*, 144–151.

(33) Ryu, S.-G.; Gruber, I.; Grigoropoulos, C. P.; Poulikakos, D.; Moon, S.-J. Large Area Crystallization of Amorphous Si with Overlapping High Repetition Rate Laser Pulses. *Thin Solid Films* **2012**, *520*, 6724–6729.

(34) Qin, G.; Fan, L.; Watanabe, A. Formation of Indium Tin Oxide Film by Wet Process Using Laser Sintering. *J. Mater. Process. Technol.* **2016**, *227*, 16–23.

(35) Zhang, Y.; Zou, G.; Liu, L.; Zhao, Y.; Liang, Q.; Wu, A.; Zhou, Y. N. Time-Dependent Wettability of Nano-Patterned Surfaces Fabricated by Femtosecond Laser with High Efficiency. *Appl. Surf. Sci.* **2016**, *389*, 554–559.

(36) Evlashin, S.; Dyakonov, P.; Khmelnitsky, R.; Dagesyan, S.; Klokov, A.; Sharkov, A.; Timashev, P.; Minaeva, S.; Maslakov, K.; Svyakhovskiy, S.; Suetin, N. Controllable Laser Reduction of Graphene Oxide Films for Photoelectronic Applications. *ACS Appl. Mater. Interfaces* **2016**, *8*, 28880–28887.

(37) Luo, J.; Jang, H. D.; Huang, J. Effect of Sheet Morphology on the Scalability of Graphene-Based Ultracapacitors. *ACS Nano* **2013**, *7*, 1464–1471.

(38) Oh, Y. J.; Yoo, J. J.; Kim, Y. I.; Yoon, J. K.; Yoon, H. N.; Kim, J.-H.; Park, S. B. Oxygen Functional Groups and Electrochemical Capacitive Behavior of Incompletely Reduced Graphene Oxides as a Thin-Film Electrode of Supercapacitor. *Electrochim. Acta* **2014**, *116*, 118–128.

(39) Arrigo, R.; Hävecker, M.; Wrabetz, S.; Blume, R.; Lerch, M.; McGregor, J.; Parrott, E. P. J.; Zeitler, J. A.; Gladden, L. F.; Knop-Gericke, A.; Schlögl, R.; Su, D. S. Tuning the Acid/Base Properties of Nanocarbons by Functionalization Via Amination. *J. Am. Chem. Soc.* **2010**, *132*, 9616–9630.

(40) Chen, C.-M.; Zhang, Q.; Zhao, X.-C.; Zhang, B.; Kong, Q.-Q.; Yang, M.-G.; Yang, Q.-H.; Wang, M.-Z.; Yang, Y.-G.; Schlögl, R.; Su, D. S. Hierarchically Aminated Graphene Honeycombs for Electrochemical Capacitive Energy Storage. *J. Mater. Chem.* **2012**, *22*, 14076–14084.

(41) Gogotsi, Y.; Simon, P. True Performance Metrics in Electrochemical Energy Storage. *Science* **2011**, *334*, 917–918.

(42) Zhang, S.; Pan, N. Supercapacitors Performance Evaluation. *Adv. Energy Mater.* **2015**, *5*, 1401401.

(43) Lin, J.; Peng, Z. W.; Liu, Y.; Ruiz-Zepeda, F.; Ye, R.; Samuel, E. L. G.; Yacaman, M. J.; Yakobson, B. I.; Tour, J. M. Laser-Induced

Porous Graphene Films from Commercial Polymers. *Nat. Commun.* **2014**, *5*, 5714.

(44) Peng, Z.; Lin, J.; Ye, R.; Samuel, E. L. G.; Tour, J. M. Flexible and Stackable Laser-Induced Graphene Supercapacitors. *ACS Appl. Mater. Interfaces* **2015**, *7*, 3414–3419.